

STRATOSPHERIC WARMINGS DURING FEBRUARY AND MARCH 1993

G. L. Manney, R. W. Zurek,

Jet Propulsion Laboratory/California Institute of Technology

A. O'Neil],

Centre for Global Atmospheric Modelling, University of Reading

R. Swinbank,

United Kingdom Meteorological Office

J. B. Kumer, J. L. Mergenthaler, A. E. Roche

Lockheed Palo Alto Research Laboratory

Abstract. Two stratospheric sudden warmings during February and March 1993 are described using UKMO analyses of height, wind and temperature, PV and diabatic heating calculated from these, and  $N_2O$  from the CLAES instrument on the UARS. The first warming affects the temperatures over a larger region, both in latitude and height, while the second produces a larger region of reversed zonal winds. During the warmings, tilted baroclinic zones form in the temperature field, and the polar vortex tilts westward with height. Large tongues of material are drawn from low latitudes into the region between the polar vortex and the anticyclone; strongest diabatic descent also occurs in this region. Narrow tongues of high PV and low  $N_2O$  are drawn off the polar vortex, and irreversibly mixed. An increase in  $N_2O$  over a broad region near the edge of the polar vortex indicates the importance of horizontal transport during these events. In the interior of the vortex,  $N_2O$  decreases, consistent with the enhanced diabatic descent during the warmings.

## Introduction

Stratospheric sudden warmings have a profound effect on the Northern Hemisphere (NH) winter stratosphere. Describing and understanding these events is essential in attempting to clarify the dynamics and transport in the NH during winter, in the following letter, we describe the evolution of the stratospheric polar vortex during two strong stratospheric warmings in the 1993 northern winter, one during late February, followed by another early in March,

## Data and Analysis

The meteorological data are geopotential heights, winds, and temperatures from the United Kingdom Meteorological Office (UKMO) data assimilation system that was developed for the Upper Atmosphere Research Satellite (UARS) project [Swinbank and O'Neil] 1993]. Rossby-Ertel potential vorticity (PV) is calculated from these data using the algorithms described by Manney and Zurek [1993]. PV fields scaled in "vorticity units", as described by Manney and Zurek [1993] will be shown in vertical cross-sections; this scaling gives a similar range of values for PV at levels throughout the stratosphere. Heating rates were calculated from UKMO temperatures and ozone from the Microwave Limb Sounder (MLS) on UARS [Waters et al. 1993], using a recent version of the radiation code first described by Shine [1987].

During the time under consideration here, the Cryogenic Limb Array Etalon Spectrometer (CLAES) on the UARS made measurements of a number of species throughout the stratosphere, including  $N_2O$ . Since  $N_2O$  has no significant stratospheric source, and its photochemical lifetime is long compared to dynamical time scales, it is an excellent tracer for transport processes.  $N_2O$  from CLAES measurements will be shown to further elucidate the motions of air during these stratospheric warmings. The utility of CLAES

$N_2O$  data for scientific purposes is described by Kumer et al. [ 1993]. The data are still in the validation process; this process has verified that the data are suitable for studies of morphology and regional variation for the north polar winter conditions addressed in this paper. The most recent UARS validation workshop, held 4 to 7 Oct 1993, resulted in typical precision and systematic error estimates of (20 ppbv rms, 20%) and (1 O ppbv rms, 20%) on the 46 and 4.6 hPa surfaces, respectively. A NASA report describing the UARS validation exercise will be issued in Dec 1993,  $N_2O$  data for a 24 h period are linearly interpolated to a regular latitude-longitude grid; ascending and descending orbit tracks are treated separately and then averaged, Both CLAES and UKMO data are interpolated to isentropic ( $f?$ ) surfaces using the UKMO temperatures, for consistency.

CLAES data extending to approximately  $80^\circ N$  are available for 12 February through 17 March 1993. UKMO data will be shown for 1 February through April to give a more complete picture of these events.

## Results

Figure 1 shows time series of zonal mean winds and temperatures, and planetary scale waves (wave 1 and wave 2) in the geopotential height field at 10 mb in the northern hemisphere for February and March 1993. The zonal mean wind reverses in the polar regions around 17 February, and in the entire region poleward of  $60^\circ N$  around 1 March. Associated with the first wind reversal is a reversal in the temperature gradient, accompanying a high latitude temperature increase of  $\approx 15$  K between 18 and 21 February. The second wind reversal is accompanied by a similar increase in temperature of  $\approx 15$  K between 2 and 5 March at high latitudes. After this second warming, the zonal mean winds return to being westerly, but the temperature gradient does not reverse back to its original sign. A gradual decrease in winds and increase in temperatures starting about the time of the first warming reflects the weakening of the polar vortex, This is typical of the

beginning of the dynamically induced final warming that usually occurs in the northern hemisphere (O'Neill and Pope, 1990). During the first warming, temperatures are affected over a broader latitude and altitude region than during the second warming, although there is a larger region of reversed winds associated with the second warming.

Figures 1c and 1d show the evolution of wave 1 and wave 2. Wave 1 is dominant during both of these warmings, reflecting the fact that the polar vortex does not split (shown below). Wave 1 is usually stationary, but during 26 February through 3 March, waves 1, 2, and 3 are in phase and move eastward with the same phase speed, reflecting the eastward motion of the polar vortex and anticyclone. Similar phase-locking frequently occurs during periods of strong wave activity in the southern hemisphere [Manney et al. 1991].

Figure 2 shows maps of PV and  $\text{N}_2\text{O}$  at 840 K, in the mid-stratosphere, for several days covering the times of the two warmings. Between 24 Feb and 5 Mar, the polar vortex and anticyclone rotate eastward by  $\approx 180^\circ$ , as suggested by the wave motions shown in Fig. 1. The vortex is much more elongated during the second warming, as shown in Fig. 1 by the amplification of wave 2 at this time. During the entire time period shown here, the polar vortex is highly distorted, as is frequently the case during the NH winter. Some low latitude air (characterized by low PV and high  $\text{N}_2\text{O}$ ) is continuously being drawn into high latitudes, into the region of the anti-cyclonic "Aleutian high". Starting on  $\approx 21$  Feb, this evolution intensifies, as a large blob of high  $\text{N}_2\text{O}$  and low PV begins to be drawn into high latitudes around the polar vortex. It is clear that low latitude air continues to be drawn into the anticyclone throughout the second warming. This air movement from subtropics into high latitudes was noted by Randel et al. [1993] for an earlier day.

In both  $\text{N}_2\text{O}$  and PV fields, there is evidence that material is being drawn off of the vortex and around the low latitude side of the high. This is particularly evident during the second warming (e. g., 5 March), when a tongue of high PV and low  $\text{N}_2\text{O}$  stretches

completely around the anticyclone. These narrow tongues that are pulled off the vortex appear to irreversibly mix, as has been noted in previous studies of stratospheric warmings [Clough et al. 1985, Leovy et al. 1985, Fairlie et al. 1990, and references therein], Excellent agreement is seen between the air motions depicted by the PV and the CLAES  $N_2O$  fields.

Figure 3 shows cross-sections of temperature and daily mean heating rates, at  $64^\circ N$  as a function of  $\theta$  and longitude, and at 840 K as a function of latitude and longitude, on 18 February and 2 March, before the peak of each warming. Although the temperature gradients appear considerably less sharp when displayed as a function of  $\theta$ , it is apparent that a baroclinic zone similar to those described by Fairlie et al. [1990], is associated with each warming. The vortex is not as strongly tilted westward with height during these warming as it was during simulations of major midwinter warmings shown by Fairlie et al, [1990] and Manney et al. [1993], so the strongest temperature gradients are in the horizontal, with vertical temperature gradients of  $\approx 3-4$  K/km (compared to 6-10 K/km in the simulations mentioned above).

Diabatic cooling is enhanced along the warm side of the baroclinic zone, due to the extreme departure of the temperatures here from radiative equilibrium, In the isentropic coordinate system, diabatic cooling is directly related to the vertical velocity, thus increased downward motion is expected in this region during the warmings. The strongest radiative cooling occurs in the region between the cyclonic vortex and the strong anti-cyclonic circulation, consistent with the temperature structure in baroclinic zones.

Figure 4 shows cross-sections of  $N_2O$  and scaled PV on 18 Feb and 2 Mar, as a function of  $\theta$  and longitude at  $64^\circ N$ , and as a function of  $\theta$  and latitude along  $0-180^\circ$  longitude (horizontal plots of  $N_2O$  on these days are shown in Fig. 2). The strongest PV gradients, which identify the position of the strong jet associated with the polar vortex, are generally between 1.2 and  $1.8 s^{-1}$ . The westward and slightly equatorward tilt of the

vortex with height is apparent. Lower  $N_2O$  values at a given level are apparent on 2 Mar than on 18 Feb along the high  $\psi$  or vortex interior side of the strong PV gradients (near  $80-100^\circ E$  longitude, for instance); this is consistent with the enhanced diabatic cooling in this region. It is much more difficult to see an effect of the enhanced vertical velocities on the extra-vortex side of this region, since that is also the region where high  $N_2O$  and low PV are being drawn into the polar regions around the anticyclone.

Figure 5 shows zonal mean  $N_2O$  near the beginning of the observing period (12 Feb) and near the end of the observing period (14 Mar), and the difference between the two. Since the two stratospheric warmings are the dominant events during this time period, it is reasonable to assume that changes in the distribution of  $N_2O$  are largely due to transport associated with these warmings. The scaled PV contours shown in Figure 5a and 5b give an idea of the location of the vortex region on these days. Over much of the stratosphere, from  $\approx 420-1300$  K,  $N_2O$  increases during the month shown, with the largest increase in the mid-stratosphere ( $\approx 900$  K), where the planetary waves also have maximum amplitude during the warmings. There is a narrow region near the pole where  $N_2O$  decreases over the period from  $\approx 420-1200$  K. A very similar pattern is seen when different days (but still near either end of the time period) are chosen.

Since  $N_2O$  generally decreases monotonically with height, and decreases poleward when the flow is relatively quiescent, it is expected that the increase is due to horizontal transport and the decrease in the polar region is due to vertical transport (diabatic descent). This is consistent with the appearance of the synoptic sections shown above, which show large amounts of material being drawn into the polar regions from low latitudes during the warmings, and evidence of descent inside the vortex in the vertical sections. Since the strongest descent is in the same region where tongues of high  $N_2O$  are being drawn in from low latitudes, the effect of this descent is not readily apparent. However, there is enhanced descent during the warmings throughout mid- to high latitudes, and this is apparent in the polar regions where horizontal transport is less dominant. The

increase in  $N_2O$  is apparently due mainly to the material that is drawn up from low latitudes around the outside of the polar vortex; the largest increase is in the vicinity of the region of strong PV gradients.

### Discussion and Conclusions

Two strong stratospheric warmings occurred during late February and early March 1993. Tilted baroclinic zones form in the temperature field, with an associated westward tilt of the stratospheric polar vortex with height, consistent with features previously noted in simulations of stratospheric warmings [Fairlie et al. 1990; Manney et al, 1993]. During the second warming the polar vortex and anticyclone travel eastward. Consistent with the behavior in simulations described by Manney et al. [1993], air from low latitudes is drawn into high latitudes around the polar vortex and into the anticyclone, and descends, as the strongest diabatic cooling also occurs in the region between cyclone and anticyclone. The  $N_2O$  fields shown here also suggest that descent is important well inside the polar vortex, where its effects are not masked by those of horizontal transport. Although there is continuous diabatic cooling in the polar regions during winter, diabatic descent is enhanced throughout the polar regions during the warmings. Evidence is also shown of narrow tongues of high PV and low  $N_2O$  being drawn off the vortex around the equatorward side of the anticyclone, and mixing irreversibly.

Excellent agreement is seen between the flow depicted by PV calculated from the UKMO data and CLAES  $N_2O$  fields, giving additional confidence in the veracity and utility of both products. Understanding the dynamics of stratospheric warmings and their effect on mixing within and around the stratospheric polar vortex is essential to diagnosing the importance of chemical and transport processes that take place in the NH polar winter stratosphere, and their effects on mid-latitudes. The UARS data and UKMO analyses shown here provide extremely valuable tools in describing stratospheric warmings

and quantifying our understanding of these events.

Acknowledgments. Thanks to the MLS team for their continued collaboration and support; to T. Luu for data management, to P. Newman for supplying routines that were adapted to calculate PV. The UARS investigation at JPL/CalTech was carried out under contract with NASA. We thank the CLAES colleagues at LPARL, Denver University, Gordley and Assoc. Tech, SW., Utah State University, and NCAR for their essential contributions to production of CLAES data in general and  $N_2O$  in particular.

#### References

- Clough, S. A., N. S. Grahame, and A. O'Neil], Potential vorticity in the stratosphere derived using data from satellites, *Q. J. Roy. Meteor. Soc.*, **111**, 335-358, 1985.
- Fairlie, T. D. A., M. Fisher, and A. O'Neil], The development of narrow baroclinic zones and other small-scale structure in the stratosphere during simulated major warmings. *Quart. J. Roy. Meteor. Soc.*, **116**, 287-315, 1990.
- Kumer, J. B., J. L. Mergenthaler, and A. E. Roche, CLAES  $CH_4$ ,  $N_2O$ , and  $CCL_2F_2$  (F12) global data, *Geophys. Res. Lett.*, **20**, 1239-1242, 1993.
- Leovy, C. B., C.-R. Sun, M. H. Hitchman, E. E. Remsberg, J. M. Russell III, L. L. Gordley, J. C. Gille, and L. V. Lyjak, Transport of ozone in the middle stratosphere: Evidence for planetary wave breaking. *J. Atmos. Sci.*, **42**, 230-244, 1985.
- Manney, G. L., J. D. Farrara, and C. R. Mechoso, The behavior of wave 2 in the Southern Hemisphere stratosphere during late winter and early spring. *J. Atmos. Sci.*, **48**, 976-998, 1991.
- Manney, G. L., J. D. Farrara, and C. R. Mechoso, Simulations of the February 1979 stratospheric sudden warming: Model comparisons and Three-dimensional

evolution. *Mon. Wea. Rev.*, *accepted, 1993*.

Manney, G. L., and R. W. Zurek, Interhemispheric Comparison of the development of the stratospheric polar vortex during fall: A 3-dimensional perspective for 1991-1992, *Geophys. Res. Lett.*, *20, 1275-1278, 1993*.

O'Neill, A., and V. D. Pope, The seasonal evolution of the extra-tropical stratosphere in the southern and northern hemispheres: Systematic changes in potential vorticity and the non-conservative effects of radiation, *Dynamics, Transport and Photochemistry in the Middle Atmosphere of the Southern Hemisphere, 33-54*, Kluwer Academic Publishers, Netherlands, 1990.

Randel, W. J., J. C. Gille, A. E. Roche, J. B. Kumer, J. L. Mergenthaler, J. W. Waters, E. F. Fishbein, and W. A. Lahoz, Stratospheric transport from the tropics to middle latitudes by planetary-wave mixing, *Nature*, *365,533-535, 1993*,

Shine, K. P., The middle atmosphere in the absence of dynamic heat fluxes. *Quart. J. Roy. Meteor. Soc.*, *113,603-633, 1987*.

Swinbank, R., and A. O'Neill, A Stratosphere-troposphere data assimilation system. *Mon. Wea. Rev.*, *in press, 1993*.

Waters, J. W., L. Froidevaux, W. G. Read, G. L. Manney, L. S. Elson, D. A. Flower, R. F. Jarnot, and R. S. Harwood, Stratospheric ClO and ozone from the Microwave Limb Sounder on the Upper Atmosphere Research Satellite, *Nature*, *362,597-602, 1993*.

#### Figure Captions

Fig. 1. (a) and (b) Zonal mean zonal wind ( $\text{m s}^{-1}$ ) and temperature (K) for 1 Feb 1993 through 1 Apr 1993, at 10 hPa. Contour interval in (a) is  $10 \text{ m s}^{-1}$ , with values from  $-10$  to  $0 \text{ m s}^{-1}$  shaded. Contour interval in (b) is 3 K, with values from 233 to 236 K

shaded. (c) wave 1 and (d) wave 2 in geopotential height (m) for same time period, Contour intervals in (c) and (d) are 100 m; 900 to 1000 m is shaded in (c) and 300 to 400 m in (d). Black dots show phase as position of one maximum,

Fig. 2. Synoptic plots of PV ( $10^{-4} \text{ Km}^2 \text{ kg}^{-1} \text{ s}^{-1}$ ) and  $\text{N}_2\text{O}$  (ppbv) at 840 K, on 18, 21, and 24 Feb, during the first warming, and on 2, 5, and 8 Mar, during the second warming. Projection is orthographic, with  $0^\circ$  longitude at bottom of plot,  $30^\circ$  and  $60^\circ$  latitude circles are shown.

Fig. 3. Temperatures (contours, K) and diabatic heating rates (colors,  $\text{Kd}^{-1}$ ) on 18 Feb and 2 Mar, (a) and (c) versus  $\theta$  and longitude at  $64^\circ\text{N}$ , (b) and (d) versus latitude and longitude at 840 K.

Fig. 4, Cross-sections of  $\text{N}_2\text{O}$  (colors, ppbv) and scaled PV (contours,  $10^{-4} \text{ s}^{-1}$ ) on 18 Feb and 2 Mar, (a) and (c) versus longitude and  $\theta$  at  $64^\circ\text{N}$ , (b) and (d) versus latitude and  $\theta$  along  $0 - 180^\circ$  longitude.  $\text{N}_2\text{O}$  continues to increase with decreasing altitude where values are off the color scale used here.

Fig. 5. (a) and (b) zonal mean  $\text{N}_2\text{O}$  (ppbv) as a function of  $\theta$  and latitude, on 12 Feb and 14 Mar; (c) the difference (ppbv) between (a) and (b). Black lines on (a) and (b) are contours of scaled zonal mean PV ( $10^{-4} \text{ s}^{-1}$ ) that approximately outline the region of strongest PV gradients, The white line in (c) is the zero contour.

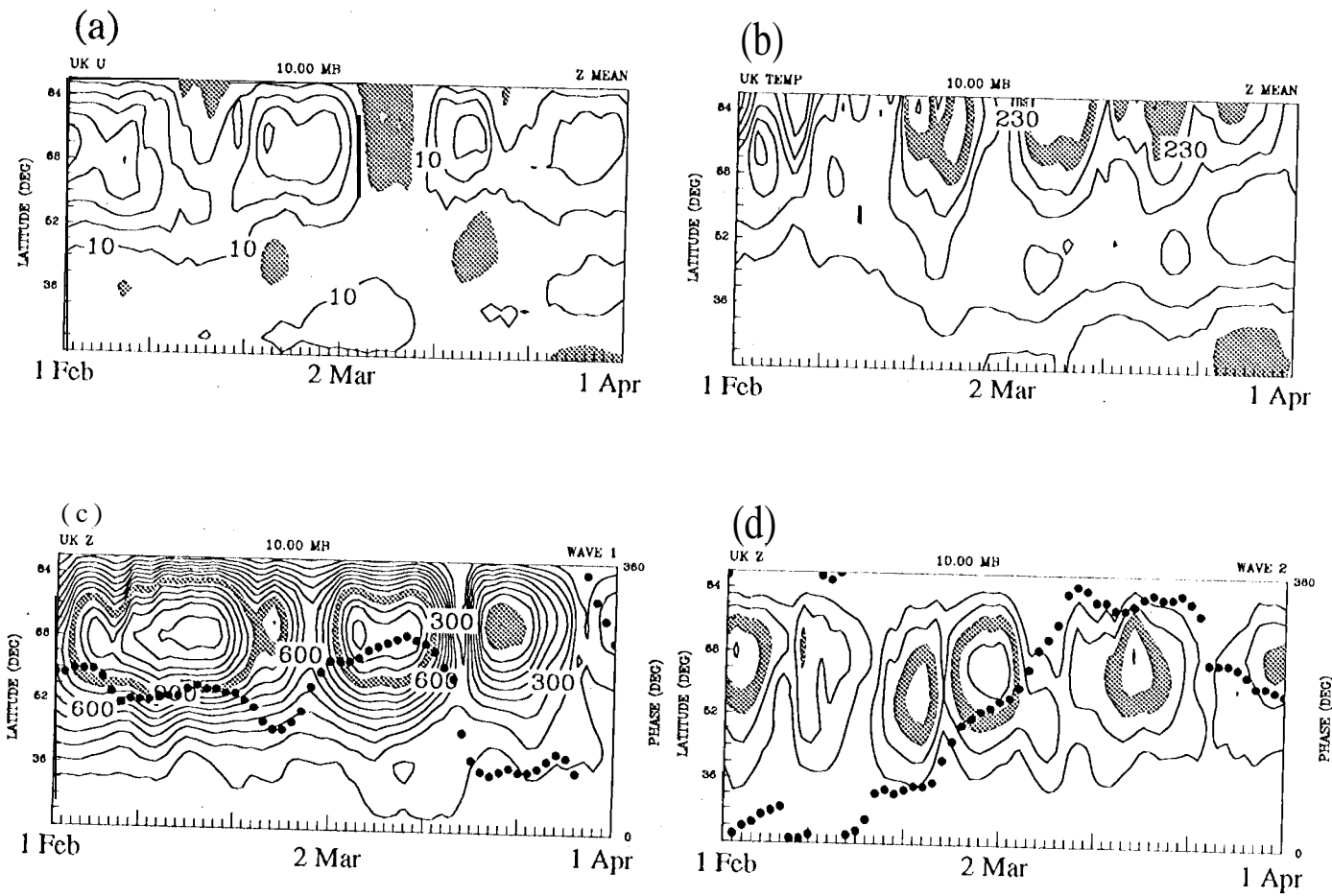


Fig. 1

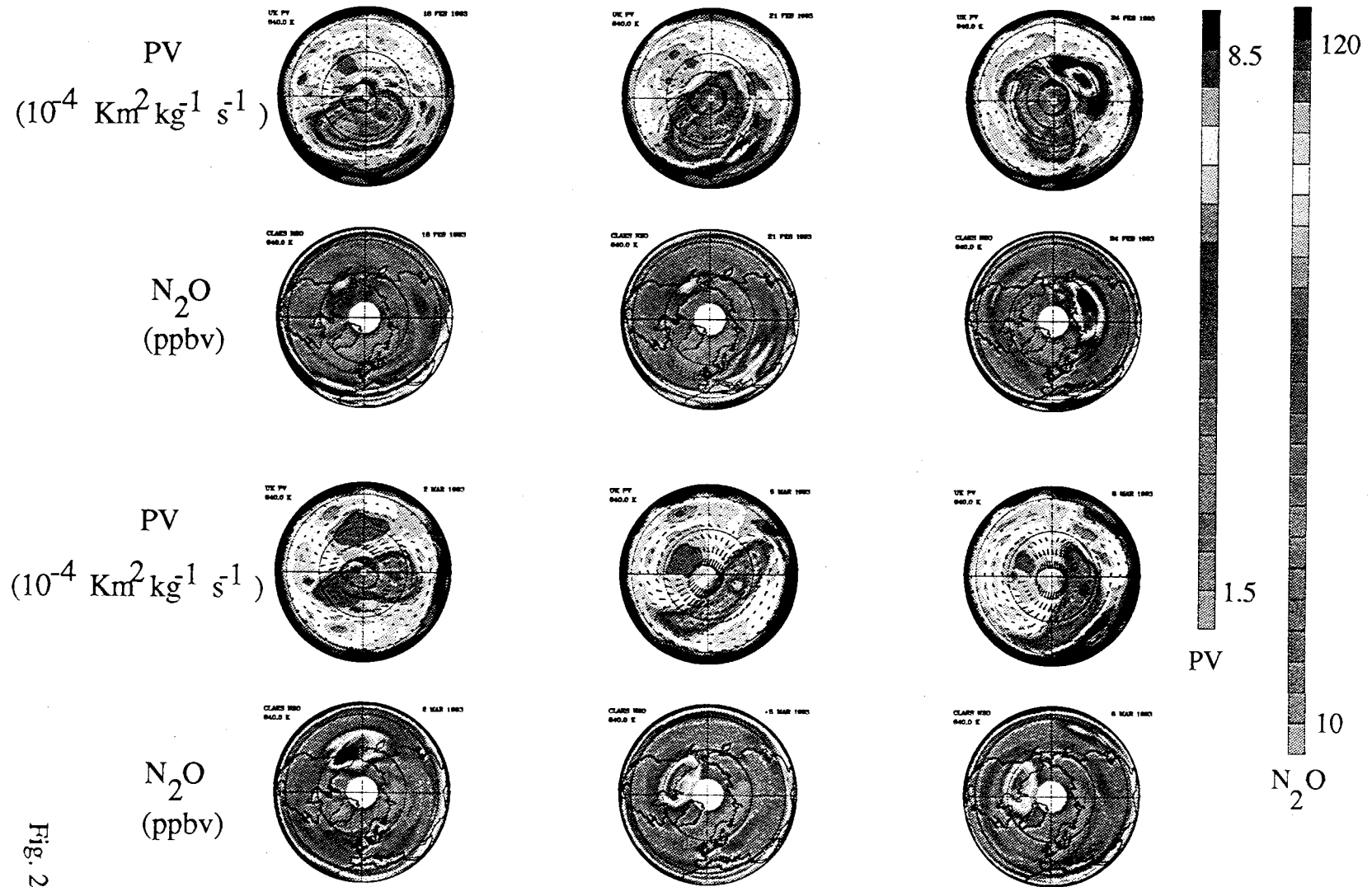


Fig. 2

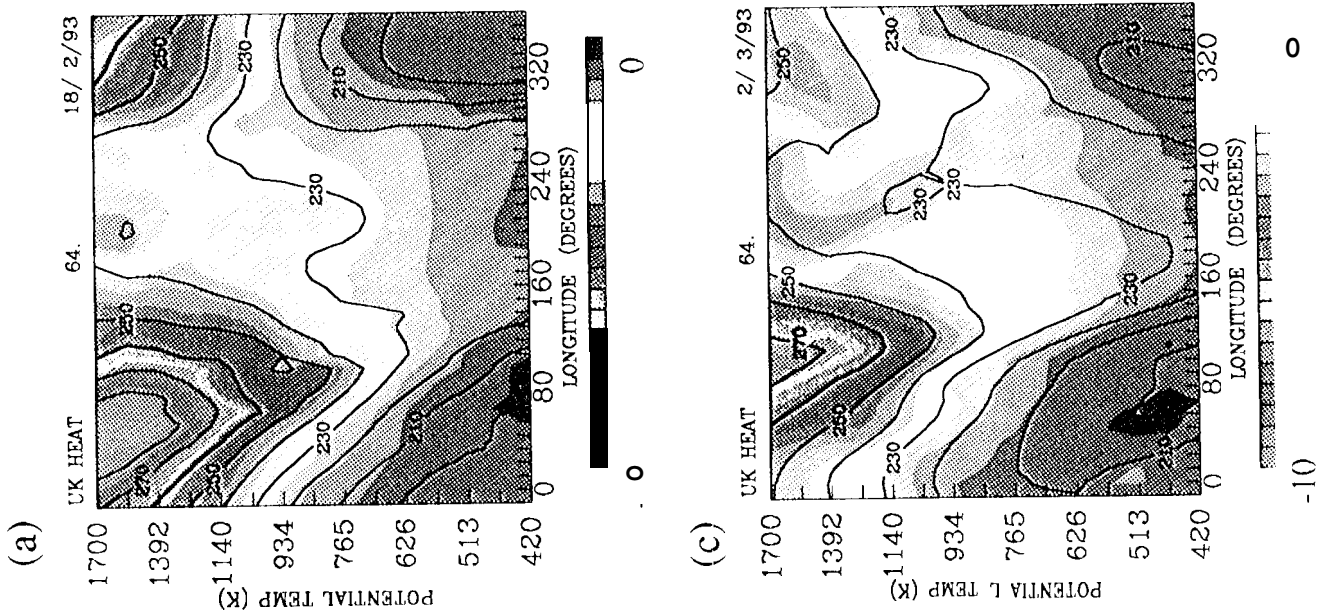
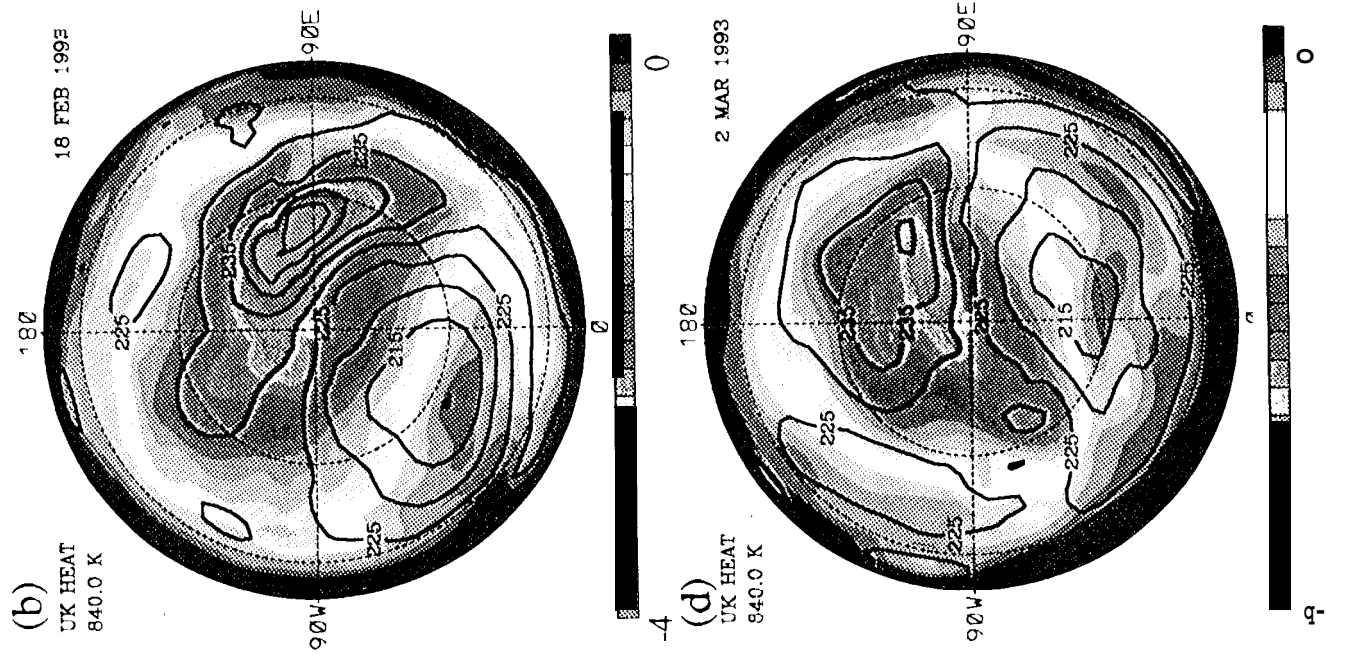


Fig. 3

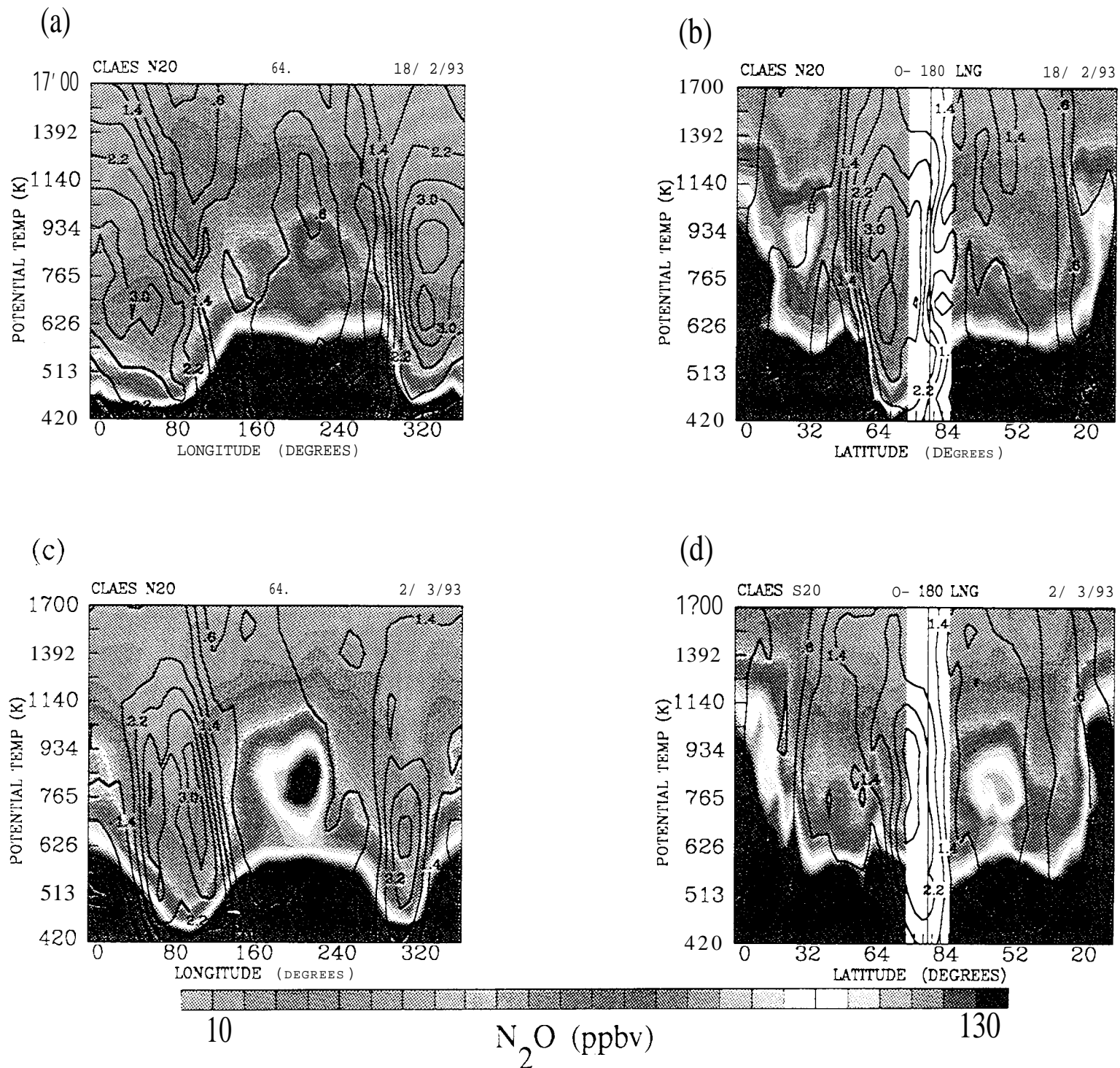


Fig. 4

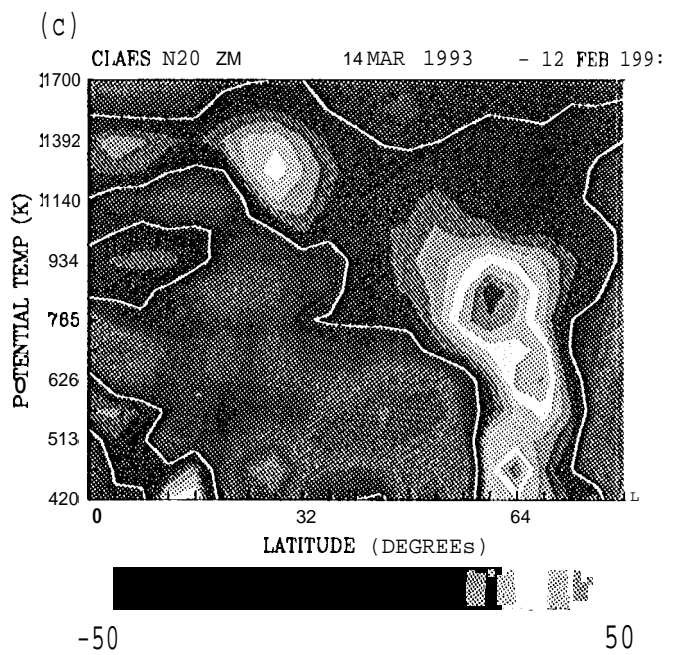
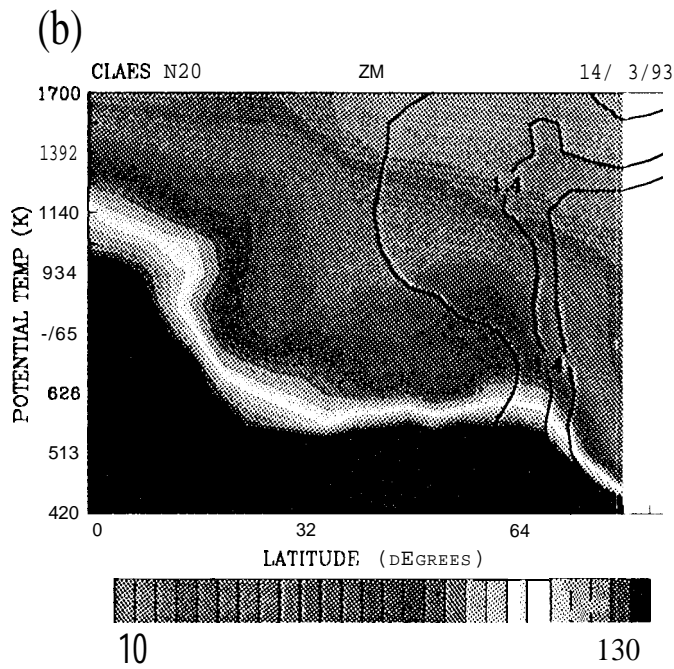
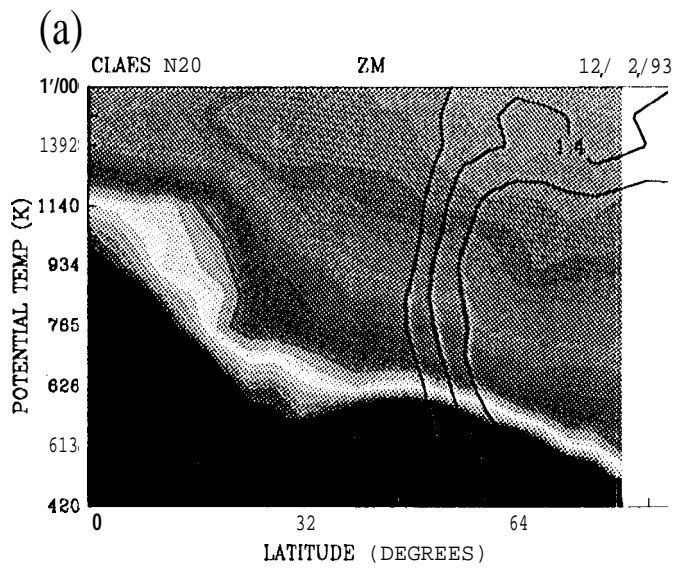


Fig 5